A Fourier-based constraint for multi-frame blind deconvolution of imagery obtained through strong turbulence

Douglas A. Hope[1] and Stuart M Jefferies[1,2,3]
[1]*Institute for Astronomy, University of Hawaii, Kula, Maui HI 96790*
[2]*Steward Observatory, University of Arizona, Tucson AZ 85721-0065*
[3]*Physics and Astronomy Department, University of New Mexico, Albuquerque NM 87131**

We demonstrate that blind restoration of an object scene from a sequence of images obtained through strong atmospheric turbulence can be significantly improved by using prior information on the distribution of the sources of regions of low spectral power (spectral holes) in the data.

I. INTRODUCTION

Blind restoration is an important post-processing technique for restoring imagery when the point spread function (PSF) for the imaging system is either not known or is poorly known. Perhaps one of the most widely used blind restoration techniques is multi-frame blind deconvolution (MFBD)[1, 2]. This technique is used for sequences of images of a target obtained over time scales such that the target can be considered stationary but the PSFs are changing. This situation is common for observations of objects through the Earth's atmosphere where fluctuations in the air temperature at the interface between different layers of air, give rise to random fluctuations in the refractive index of the air. These fluctuations then produce aberrations in any wave front propagating through the air (hence yielding a changing PSF).

The blind restoration problem is typically both ill-conditioned (due to noise in the measurements) and ill-posed(i.e. it does not have a unique solution[3]). However, one can find physically meaningful solutions by using prior information about the object being viewed (e.g., spatial extent, positivity, real-plane zeros[4]) and knowledge about the underlying physics of the imaging process. In general, the fidelity and resolution of the restoration is directly related to the amount and quality of prior information used to constrain the restoration. Here we investigate a new information prior that is based on the fact that not all spatial frequencies in the data carry the same amount of information.

We restrict our studies to imagery that is obtained under isoplanatic conditions, that is, the PSFs are spatially invariant. This allows us to describe the observed imagery $g_k(\mathbf{x})$ in terms of a convolution of the target object $f(\mathbf{x})$ and PSF $h_k(\mathbf{x})$ plus additive noise $n_k(\mathbf{x})$. That is,

$$g_k(\mathbf{x}) = f(\mathbf{x}) \odot h_k(\mathbf{x}) + n_k(\mathbf{x}) \tag{1}$$

where the subscript k denotes a time index. Equivalently, the observed Fourier spectra are represented by

$$G_k(\mathbf{u}) = F(\mathbf{u})H_k(\mathbf{u}) + N_k(\mathbf{u}) \ . \tag{2}$$

Isoplanatic conditions will apply when the main source of atmospheric turbulence is close to the telescope aperture.

II. SPECTRAL HOLES

Spatial frequencies in the data that have low Fourier power carry little or no information. We refer to such frequencies as *spectral holes*. Equation (2) shows that, in spectral regions where the signal-to-noise ratio is greater than unity, spectral holes in the data are a direct result of holes in the spectra of the object and PSF. In general, the source of an individual hole is unknown. However, when imaging a stationary object through the turbulent atmosphere, the spectral holes in the data associated with the PSF will change from frame to

*Electronic address: dhope@ifa.hawaii.edu

frame while the holes that are part of the object spectrum will remain fixed. This allows us to identify the source of each hole and thus determine the distribution of the spectral holes between the PSF and object.

Interestingly, the Fourier spectra of man-made objects such as spacecrafts and satellites appear to have a large fraction of the spectrum that can be omitted before any significant visual impact is noticed (see Figs. 1 and 2).

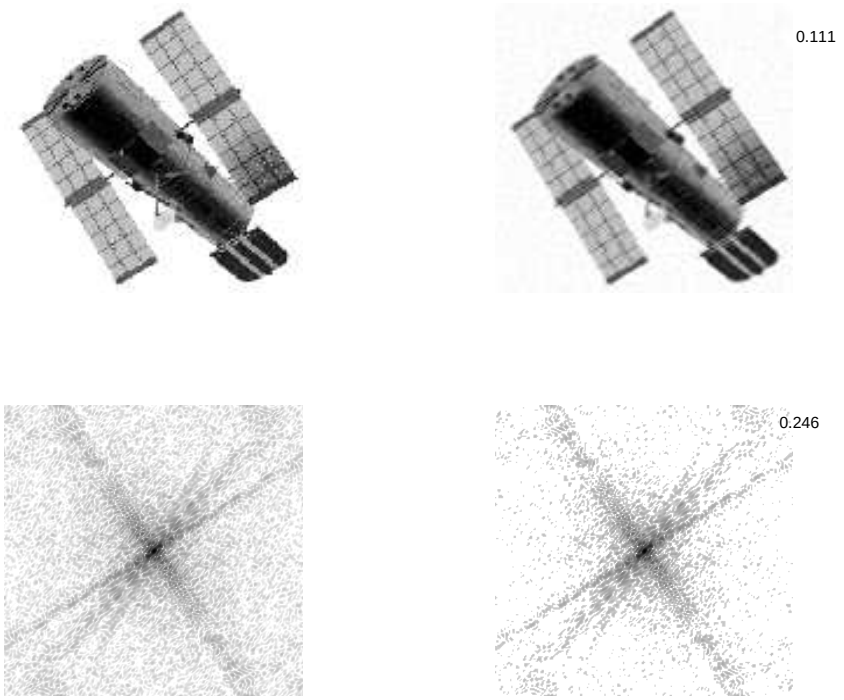

FIG. 1: Left column: Model of the Hubble Space Telescope [top] and its full Fourier spectrum [bottom]. Right Column: Fourier-constrained object where the threshold for identifying spectral holes is 10^{-5} the peak object power. The number in the upper right hand corner of the top panel denotes the relative r.m.s. error[a] between the constrained target and the truth, while the number in the bottom panel denotes the fractional amount of the Fourier spectrum that is non-zero.

[a]The relative root mean square (r.m.s.) error between the truth and the Fourier-constrained scene is defined as

$$\sigma = \left(\frac{\sum_{\mathbf{x}} [f(\mathbf{x}) - f^c(\mathbf{x})]^2}{\sum_{\mathbf{x}} f(\mathbf{x})} \right)^{1/2},$$

where $f(\mathbf{x})$ is the truth object, and $f^c(\mathbf{x})$ is the Fourier-constrained target scene, that is the scene after spectral holes are excluded from the spectrum.

Knowing the locations of these regions of low power (spectral holes) should therefore provide a strong prior constraint on the object during the image restoration process. Similarly, knowledge of the spectral hole structure for the PSF should aid in the recovery of the PSF. The leverage gained from using this prior information on the PSF, however, will depend on the strength of the turbulence and the extent of the power spectrum of the object. The former is because the number of PSF spectral holes increases as the turbulence strength increases (see Figs. 3 and 4). The latter is a consequence of how we identify PSF spectral holes (see below), basically they can only be identified in regions where the object spectrum has signal.

Our method for identifying the sources of the observed spectral holes relies on the fact that for a sufficiently large data ensemble, the average power spectrum of the PSFs is expected to be nonzero out to the diffraction-limit of the observations[5]. With this assumption we compute the ensemble SNR,

$$SNR^n(\mathbf{u}) = \sqrt{n} \frac{\langle |G(\mathbf{u})|^2 - |N(\mathbf{u})|^2 \rangle}{\sigma_G}, \tag{3}$$

where n denotes the number of frames and σ_G denotes the error due to the random nature of atmospheric turbulence. The noise bias $|N|^2$ is estimated from spatial frequencies beyond the diffraction cut-off frequency.

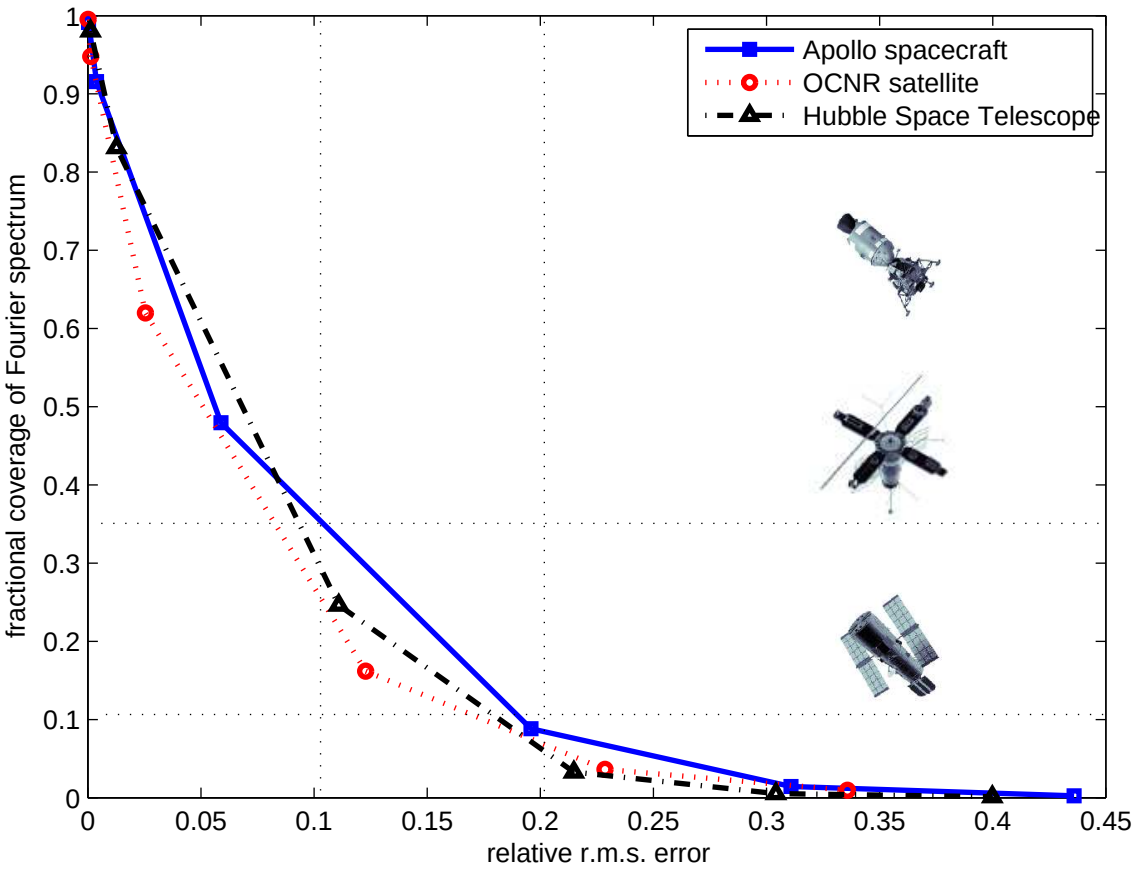

FIG. 2: The r.m.s. error for three different man-made targets as the value of threshold that identifies a frequency as being spectral hole is changed. Visually noticeable changes typically appear when the r.m.s. error values are between 0.1 and 0.2

We then define a spectral frequency as being an object spectral hole if the power at that frequency is below some user set threshold T_F. One basis for setting the value of, T_F, is that it should equal some minimum value of SNR.

Once the object holes are known the PSF spectral holes can be computed for each frame using the individual frame SNR,

$$SNR(\mathbf{u}) = \frac{\langle |G(\mathbf{u})|^2 \rangle}{\sigma_N}, \tag{4}$$

where σ_N denotes the standard deviation of the additive noise-process. Spatial frequencies in frames where $SNR(\mathbf{u})$ is below the threshold T_H (again defined in terms of local SNR) are then associated with spectral holes of the PSF. It is obvious that we can only identify PSF spectral holes where there is signal in the spectrum of the object. This means that we usually only have knowledge of a subset of the PSF spectral holes. Finally, we note that spectral holes can only be cleanly identified in data when the target signal is completely captured by the imaging array. Any truncation of the signal by the detector array will lead to artificial zeros in the Fourier spectra of the observed data.

III. MFBD ALGORITHM USING SPECTRAL HOLES

We model the object and PSF intensity distributions using the generic prescription[6]

$$a(\mathbf{x}) = \phi(\mathbf{x}) \cdot \phi(\mathbf{x})^* \tag{5}$$

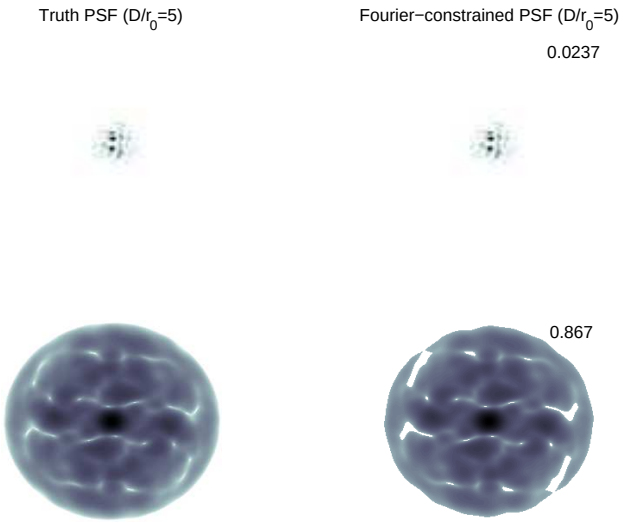

FIG. 3: Left column: Truth PSF for $D/r_0 = 5$ [top] and its Fourier spectrum [bottom] Right column: Fourier constrained PSF [top] where spectral frequencies with power below 10^{-4} have been identified as spectral holes. The number in the upper right corner is the relative error between the truth and the constrained PSF while the number in the lower right is the fraction of frequencies within the PSF band-limit that remain after applying the threshold.

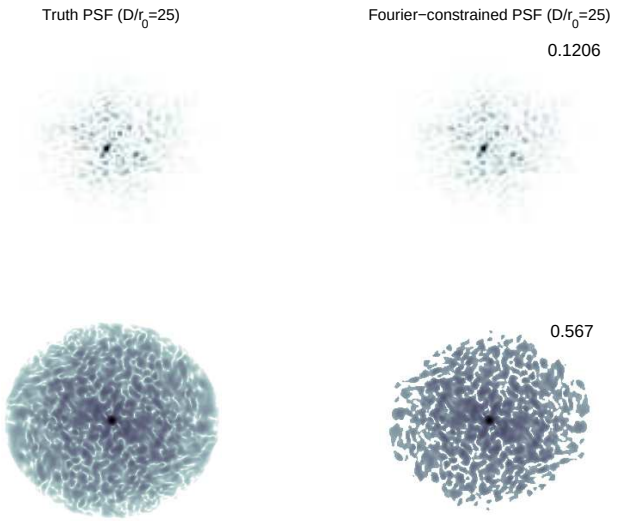

FIG. 4: Left column: Truth PSF $D/r_0 = 25$ [top] and its Fourier spectrum [bottom] Right column: Fourier constrained PSF [top] where spectral frequencies with power below 10^{-4} have been identified as spectral holes. The number in the upper right is the relative error between the truth and the constrained PSF while the number in the lower right is the fraction of frequencies within the PSF band-limit that remain after applying the threshold.

which enforces our prior knowledge that both functions must be real and positive. The variables of this model can be defined in either the image domain or in the Fourier domain. In the latter case we use the reparameterization

$$\begin{aligned} \phi(\mathbf{x}) &= F^{-1}\{\Phi(\mathbf{u})M(\mathbf{u})\} \\ &= F^{-1}\{P(u)e^{i\theta(u)}\} \end{aligned} \tag{6}$$

where F^{-1} denotes the inverse Fourier Transform, $P(\mathbf{u}) = M(\mathbf{u})|\Phi(\mathbf{u})|$, $\theta(\mathbf{u}) = \tan^{-1}(\Im\{\Phi(\mathbf{u})\}/\Re\{\Phi(\mathbf{u})\})$, $M(\mathbf{u})$ is a real-valued binary mask that is defined over the central N/2 x N/2 region of the pixel array used

to model $\Phi(\mathbf{u})$, N is the number pixels in the array and * denotes the complex conjugate.

Here we choose the image domain approach for modeling the object (i.e. $\phi(\mathbf{x})$ are the variables) and the Fourier domain approach for modeling the PSFs (i.e., $P(\mathbf{u})$ and $\theta(\mathbf{u})$ are the variables). The choice was based on the fact that the latter version of the model directly incorporates the physics of the imaging system - $P(\mathbf{u})$ and $\theta(\mathbf{u})$ represent wave-front amplitudes and phases, respectively, and $M(\mathbf{u})$ incorporates information on the pupil of the telescope - while the former version allows prior knowledge of the morphology of the object to be straightforwardly incorporated into the deconvolution problem. In this work we ignore the effects of scintillation (variations in the wave-front amplitudes) and only estimate variations in the wave-front phases.

The variables in the image model are determined using a conjugate gradient algorithm to minimize the cost function

$$\epsilon = \Sigma_j \alpha_j \epsilon_j \tag{7}$$

where the individual components ϵ_j represent the enforcement of different prior information. For this work we have three terms (j=3), ϵ_0 which measures the error between the data model and the actual data, while ϵ_1 and ϵ_2 penalize energy at spatial frequencies defined to be spectral holes in the object and PSF respectively. The ϵ_0 component is given by

$$\epsilon_0 = \sum_k \sum_{\mathbf{x}} r_k^2(\mathbf{x}), \tag{8}$$

where ϵ_0, and

$$r_k(\mathbf{x}) = d_k(\mathbf{x}) \frac{\hat{g}_k(\mathbf{x}) - g_k(\mathbf{x})}{[\hat{g}_k(\mathbf{x}) + \sigma_N^2]^{1/2}}. \tag{9}$$

Here $d_k(\mathbf{x})$ is a binary *data* mask with zeros at locations of bad pixels or pixels with a low image domain SNR and $g_k(\mathbf{x})$ represents the observed data at different times (k). In the denominator, $\hat{g}_k(\mathbf{x})$ and σ_N, represent the Gaussian and Poisson components of the noise variance respectively[7]. The ϵ_j components are given by

$$\epsilon_j = \sum_k \sum_{\mathbf{u}} M_k^{\text{hole}} |\hat{A}_k(\mathbf{u})|^2, \tag{10}$$

where $A(\mathbf{u})$ is the Fourier transform of $a(\mathbf{x})$.

We note that, ideally, the ϵ_j should mimic a probability density function so that $\alpha_j = 1$ for all j. However, it is not always practical to achieve this requirement and values of α_j need to be determined that will provide the best solution. Here we define $\alpha_0 = 1$ and choose the values of $\alpha_{j\neq 0}$ such that the derivatives $\partial\epsilon_j/\partial\theta(\mathbf{u})$ are all similar in magnitude at the beginning of the iteration. We have found that this results in values for α_j that are close to optimal.

IV. RESULTS AND DISCUSSION

For this work we simulated several sets of 100 speckle data frames to represent imaging through a variety of turbulence strengths. The details of how the data were simulated are given in the appendix. We identified the object and PSF spectral holes for each data set using all 100 frames.

We found that for weak turbulence the quality of the image restorations with and without the spectral hole prior were almost identical. However, for strong turbulence we found that the image restorations with spectral holes provided significant improvement over those without spectral holes, e.g. see Fig. 5.

For some imaging scenarios the object may remain stationary for long periods of time, e.g. geo-stationary targets, and the data sets acquired may run to thousands of frames. Although the computational burden associated with identifying spectral holes from such a large data set is negligible, the burden associated with the MFBD restoration of the full data would, however, be extremely large. For this reason we have examined the use of spectral holes identified from a large number of frames to constrain the MFBD restorations of a smaller subset of the data, e.g. see Fig 6. Here knowledge of the object and PSF spectral holes was computed from the entire 100 frames and then used in an MFBD restoration using only 20 frames. Though the quality of these restorations is below that of those shown in Fig. 5, the time needed to compute the restoration is a small fraction of the time needed when using all 100 frames.

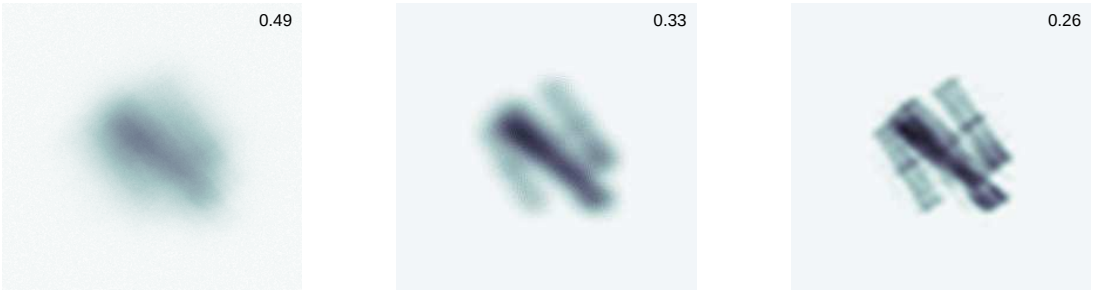

FIG. 5: Left: raw speckle frame of HST for $D/r_0 = 25$. Middle: Image restoration using 100 frames but no information about the distribution of the spectral holes. Right: Restoration using 100 frames and knowledge of the spectral holes.

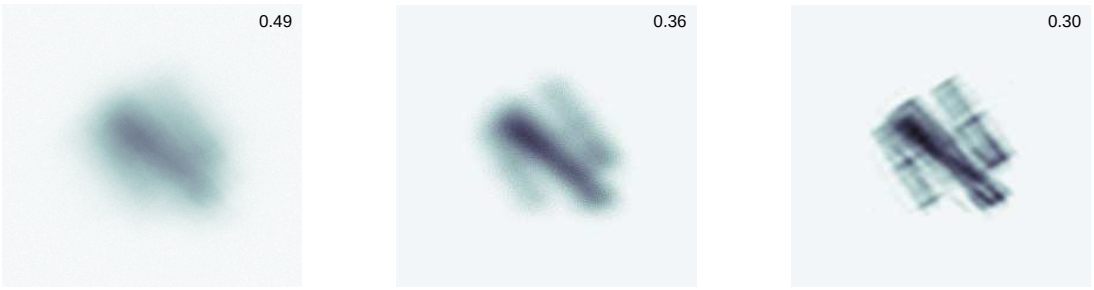

FIG. 6: Left: raw speckle frame of HST for $D/r_0 = 25$. Middle: Image restoration using 20 frames but no information about the distribution of the spectral holes. Right: Restoration using 20 frames with knowledge of object and PSF spectral holes estimated from the entire 100 frames.

We note that in addition to reducing the sensitivity of the MFBD algorithm to entrapment in local minima during the minimization process, penalizing the presence of power at the object and PSF spectral hole locations also provides a natural way to regularize against noise artifacts that typically appear at large iteration numbers (which are required to restore the high-frequencies in the object and PSFs). This is demonstrated both in Figs. 1, 2 and 4 where the distortion to the morphologies of "Fourier-constrained" satellite-type objects and PSFs for strong turbulence is relatively small despite a large fraction of their spectra being constrained to be zero, and in the restorations (using spectral holes) shown in Figs. 5 and 6 which clearly show that the restored object is regularized without sacrificing high-frequency information.

In summary our experiments indicate that when the target signal is completely captured by the imaging detector, spectral holes should be used as a constraint when performing MFBD restoration of imagery obtained through strong turbulence.

Acknowledgements: This work was performed under awards F9550-06-1-0179 and F49620-02-1-0107 from the Air Force Office of Scientific Research. The restorations were performed on computers at the Maui High Performance Computing Center (MHPCC), award F29601-01-D-0083. Michael-Lloyd Hart provided the target scenes (Apollo and Hubble Space Telescope).

APPENDIX A: SIMULATION OF SPECKLE DATA

We generated random wavefronts using a Karhunen-Loeve (KL) expansion of Zernike polynomials[8]. We simulated tip/tilt correction by computing and subtracting out the tip/tilt low order modes from each wavefront. We then verified that our wavefronts followed the Kolmogorov turbulence model by comparing the computed short exposure structure function to the approximate analytic structure function[9]. The simulated speckle PSF is then computed using Eqs. 5 and 6, where $M(\mathbf{u})$ denotes the telescope pupil.

[1] Jefferies, S. M. and Christou, J. C., "Restoration of Astronomical Images by Iterative Blind Deconvolution," Astrophys. J. , **415,** 862 (1993)
[2] Schulz, T. J., "Multi-frame blind deconvolution of astronomical images," J. Opt. Soc. Am. A, 10, 1064-1073 (1993).
[3] Tikhonov, A. N.and Arsenin, V. Ya., Methods for Solving Ill-posed problems, Nauka, Mosco W. (1979)
[4] Chen, P., Fiddy, M. A., Liao, C. W. and Pommet, A., "Blind deconvolution and phase retrievel from point zeros," J. Opt. Soc. Am. A, 15, 7, 1996.
[5] Labeyrie, A., "Attainment of Diffraction Limited Resolution in Large Telescopes by Fourier analyzing Speckle Pattersn in Star Images," Astron. Astrophys. **6**, p. 85 (1970)
[6] Miura, N., "Blind deconvolution of band limited images," Optics Letter. **28**, p. 2312-2314 (2003)
[7] Jefferies, S. M., M.Lloyd-Hart, E. K. Hege, and J. Georges, "Sensing wave-front ampltiude and phase with phase diversity," Applied Optics **41**, 11 p. 2095-2102. (2002).
[8] Roddier, N., "Atmospheric wavefront simulation using Zernike polynomials," Optical Engineering **29**, 10 p. 1174–1180 (1990).
[9] Fried, D. L., "Optical resolution through a randomly inhomogeneous medium for very long and very short exposures," J. Opt. Soc. Am. A **56,** 1372–1379 (1966).